Thermal Rate Coefficients via Variational Transition State Theory for the Unimolecular Decomposition/Isomerization of 1-Pentyl Radical: Ab Initio and Direct Dynamics Calculations

Luminita C. Jitariu,[†] Lee D. Jones,[†] Struan H. Robertson,[‡] Michael J. Pilling,[§] and Ian H. Hillier*,[†]

Department of Chemistry, University of Manchester, Oxford Rd, Manchester, M13 9PL, U.K., Accelrys, 240/250, The Quorum, Barnwell Rd, Cambridge, CB5 8RE, U.K., and School of Chemistry, University of Leeds, Leeds, LS2 9JT, U.K.

Received: April 1, 2003; In Final Form: July 30, 2003

Calculations of thermal rates for the reactions of the isomeric pentyl radicals involving (1,2), (1,3), (1,4), and (1,5) intramolecular H-atom transfer, C−C bond scission, and H-atom elimination have been carried out. Potential energy surfaces and associated properties for these reactions have been used for direct dynamics studies within conventional and variational transition state theory formalism including nonclassical effects, using the dual-level technique (PUMP-SAC2/6-311G**///AM1). We found that for C−C scission, the barrier is broad, and a significant tightening of the loose transition state reduces the rate coefficients across a wide temperature range. Converse behavior is predicted for the isomerization reactions where the optimal combination of a low effective mass with a narrow barrier opens the best tunneling paths. High-pressure limiting rate coefficients and kinetic parameters obtained in this study show good agreement with experimental measurements and previous theoretical work.

1. Introduction

An understanding of the kinetic behavior of alkyl radical reactions is central for modeling the overall oxidation process of large alkanes, yet the kinetic databases lack well-defined rate parameters for many of the elementary steps required for such combustion models. The overall motivation of this present study is the need to carry out the practical modeling of chemical systems when experimental rate data are fragmentary or absent.

Several reactions involving large alkanes generate alkyl radicals that can dissociate, isomerize, or react with oxygen. At low temperature, alkyl radicals react primarily with O_2 to form peroxy radicals, thus initiating chemistry typical of the autoignition regime.[1] At higher temperature, in alkane flames, isomerization and decomposition (C−C fission) of the alkyl radicals become competitive with reaction with O_2, substantially affecting the autoignition characteristics. Isomerization is rarely an important process for small radicals, due to the constrained transition state for the intramolecular hydrogen shift, whereas for larger radicals, such as pentyl, isomerization occurs with lower activation energy than dissociation.

The pressure dependence of the rate coefficients becomes more important at higher temperature so that it must be adequately incorporated into models developed for complex chemical systems. A combination of theory and experiment has been employed in studies of alkyl,[2−4] alkoxy,[5,6] and halogenated alkoxy radicals,[7] which are important in atmospheric and/or combustion chemistry. Accurate direct measurements have been made for the unimolecular decomposition of small alkyl radicals[8] at low pressure where such reactions are in the falloff region. However, the experimental data for larger radicals are limited to experimentally accessible conditions, so that theoretical studies are valuable in providing data that cannot be readily obtained through experiment. The potential energy surface (PES) routinely obtained through quantum chemical calculations provides the key to determining the reaction kinetics. The geometries, vibrational frequencies and energies of stationary structures can be combined with statistical theories (e.g. transition state theory (TST)[9] and variational transition state theory (VTST)[10]) to calculate kinetic parameters. Modeling of a complex system that can isomerize by multiple pathways and fragment by C−C or C−H bond breakage in competition with collisional stabilization, can be accomplished using master equation (ME) simulations to derive the overall macroscopic rate constants. ME methods have been developed and tested to model the pressure dependence of the rate coefficient of simple (single well)[11,12] unimolecular reactions and recent work has extended their application to multiwell systems.[13−15]

The 1-pentyl system (1-C_5H_{11}) is essentially a two-well system with a low isomerization threshold to secondary radical (2−C_5H_{11}) formation. Dissociation occurs from both radicals, primarily via C−C rather than C−H bond cleavage, to produce radical + alkene products, according to the following reaction scheme:

$$C_3H_7 + C_2H_4 \leftarrow 1\text{-}C_5H_{11} \leftrightarrow 2\text{-}C_5H_{11} \rightarrow C_3H_6 + C_2H_5 \quad (1)$$

This system has been investigated experimentally using both steady state and shock tube techniques.[16−23] Modeling studies of Tsang and co-workers,[24] using a master equation technique, have also revealed the complex time dependence in the evolution of the 1-pentyl system at higher temperatures (1000−2000 K, $p = 0.1$ bar).

The aim of the present work is to calculate the overall PES using ab initio molecular orbital calculations and to perform dynamics calculations for the elementary steps of the 1-pentyl system, including isomerization to the secondary radical and

[†] University of Manchester.
[‡] Accelrys.
[§] University of Leeds.

10.1021/jp034843z CCC: $25.00
Published on Web 09/12/2003

decomposition of both radicals via C−C bond cleavage. Barrier heights are compared with previously reported data to test the reliability of various theoretical models applied in this work. A method is then selected that is both accurate and computationally economic to calculate the rate coefficients in the high-pressure limit using variational transition state theory with the inclusion of multidimensional tunneling. Both the thermodynamic data calculated for the reacting species, as well as these rate coefficients are needed to evaluate the phenomenological rate constants, which will be described in a subsequent paper.

2 Computational Details

2.1. Ab Initio Calculations. To calculate rate coefficients for isomerization and decomposition of 1-pentyl radical, we start with the initial exploration of the ground state PES. The geometries of the stationary points were initially located at the semiempirical AM1 level followed by the UMP2(Fc)/6-311G** level, where the effect of dynamical electron correlation is included through second-order Møller−Plesset perturbation theory (Fc denotes the frozen-core algorithm). Standard basis sets including polarization and diffuse functions, such as 6-311G** and 6-311++G** were used. Each stationary point was characterized as a minimum or transition state through normal-mode analysis and to obtain the zero-point vibrational energy (ZPE) and thermal corrections to the molecular energy. Intrinsic reaction coordinate (IRC) calculations were carried out on all transition states to confirm the connection between the reactants and products. The IRC analysis also showed that two of the cyclic transition states for isomerization (1,4- and 1,5-H shift) lead to rotational conformers of higher energy, thus requiring a consideration of conformational energetics. The geometry optimization for each open-shell species was carried out with no symmetry constraints, the orbitals used in the UMP2 calculations being obtained from UHF calculations in all cases. As a measure of the spin contamination we found that the expected value of S^2 ranges from 0.76 to 0.81 for the parent radicals and for the saddle points for intramolecular H-atom transfer. The effect is somehow larger at the saddle points for C−C bond dissociation, where $\langle S^2 \rangle$ has a value of 0.91. The effect of spin contamination on the energetics can be taken into account using spin projection methods. To see the effect of spin contamination on the molecular geometries subsequently used in the dynamics calculations, we use a multireference wave function. Thus the geometries of the parent radicals and saddle points for decomposition were reoptimized using a complete active space−SCF (CASSCF) wave function.[25] To account for the nondynamic electron correlation, calculations at the CASSCF-(3,3)/6-311G** level were used. The choice of the size of the configuration-space is based on examination of the occupancy of the natural orbitals at the UHF/6-311G** level. The new geometries of the saddle points for decomposition, at the CASSCF(3,3)/6-311G** level of theory, are consistent with those predicted by the UMP2/6-311G** level so we conclude that a single-reference treatment provides a fairly good description of the electronic structure. If not otherwise stated, all theoretical data reported hereafter refer to the UMP2/6-311G** optimized structures. We considered the following levels of theory in our rate constant calculation: AM1, PUMP2/6-311G**, PUMP2/6-311++G**, and PUMP-SAC2/6-311G** where P denotes the projected UMP2 energy which is known to give more reliable results for open-shell systems than the MP2 methods.[26]

The MP-SAC2 method[27] (Møller−Plesset second-order-scaling all correlation energy) does not accurately estimate the correlation energy, which is taken to be the difference between the experimental and the Hartree−Fock dissociation energy, and is accounted for by a factor F_2

$$F_2 = \frac{D_e(\mathrm{MP2}) - D_e(\mathrm{HF})}{D_e(\mathrm{exp}) - D_e(\mathrm{HF})} \tag{2}$$

which represents the fraction of the valence correlation energy recovered by MP2 and the basis set for a given bond type. In this approach, the MP2 method describes the correlation effects with the same accuracy for different geometries for a given system and can also be assumed to hold among several systems. The factor F_2 is constant over a given PES[27] and consequently the total energy is written as

$$E_{\mathrm{PUMP-SAC2}} = E_{\mathrm{PUHF}} + \frac{E_{\mathrm{PUMP2}} - E_{\mathrm{PUHF}}}{F_2} \tag{3}$$

Values of F_2 were reported for homo- and heteronuclear bonds, including the C−H and C−C bonds, by Truong and Truhlar[28] and Gordon and Truhlar,[29] respectively. We use values of $F_2 = 0.84$ and $F_2 = 1.02$ for C−H and C−C respectively, as deduced for a 6-311G** basis set, which suggest that the extent of the recovery of the correlation energy achieved by the MP2/6-311G** model is 84% in the case of the C−H bond and is slightly overestimated for the C−C bond. The formulation given by eq 3 is modified from the original due to the inclusion of the projected PUMP2 and PUHF energies. All electronic structure calculations were carried out using the Gaussian98 program[30] and rate calculations used the Gaussrate program.[31]

2.2. Dynamics. The canonical high-pressure limiting rate coefficients $k(T)$ were calculated using generalized transition state theory (GTST)[10] in both conventional (TST) and canonical variational (CVT) forms**.** We briefly outline a few steps in the calculation of $k(T)$ including the tunneling contribution to allow a later discussion of the features of the PES which are critical in determining the overall kinetics. Details of the CVT and tunneling methods have been described elsewhere.[32−35] The rate constant $k(T)$ is calculated using

$$k(T) = \kappa \frac{k_B T}{h} \exp\left(-\frac{\Delta G_T^{\#}}{RT}\right) \tag{4}$$

where $\Delta G_T^{\#}$ is the free energy of activation and κ is a transmission coefficient based upon the use of a semiclassical tunneling approximation, either zero-curvature minimum-energy path (ZCT)[34] or centrifugal dominant small-curvature (SCT)[35] model. For both, the effective potential for tunneling is given by the adiabatic ground-state potential, $V_a^G(s)$:

$$V_a^G(s) = V_{\mathrm{MEP}}(s) + \sum_{i=1}^{3N-7} \frac{1}{2} h\nu_i(s) \tag{5}$$

where $V_{\mathrm{MEP}}(s)$ is the potential energy along the minimum energy path (MEP) and $\nu_i(s)$ are ground-state vibrational modes orthogonal to the reaction coordinate s. The transmission coefficient is obtained from the ratio of the Boltzmann averaged quantal and classical transmission probabilities through the effective potential

$$\kappa(T) = \frac{\int_0^\infty P(E) \exp\left(-\frac{E}{k_B T}\right) \mathrm{d}E}{\int_{V_a^G(s^{\mathrm{CVT}})}^\infty \exp\left(-\frac{E}{k_B T}\right) \mathrm{d}E} \tag{6}$$

TABLE 1: Energy Differences[a] ($E_{TS} - E_R$) for Different Unimolecular Reactions for 1-Pentyl and 2-Pentyl Radicals[b]

	reaction									
method	R1	R2	R3	R4	R5[g]	−R1	−R2	−R3	−R4	R7[g]
AM1	38.6	39.7	24.6	19.6	35.5	43.8	44.5	29.8	19.6	36.5
PUMP2/6-311G**	41.2	40.5	23.4	18.3	33.1	43.5	42.5	25.7	18.3	32.6
PUMP2/6-311++G**	40.4	40.3	23.7	18.6	32.8	42.6	42.2	25.9	18.6	32.1
PUMP−SAC2/6-311G**	39.3	38.4	21.2	15.9	32.8	41.6	40.4	23.5	15.9	32.4
G2(MP2)					32.0					31.9
G2(PMP2)					32.1					32.0
contribution of ZPE										
ΔZPE[c]	−1.8	−2.0	−1.5	−1.4	−2.5	−1.9	−2.0	−1.6	−1.4	−2.8
ΔZPE[d]	−2.3	−2.4	−2.1	−1.7	−1.5	−2.3	−2.7	−2.2	−1.7	−2.0
ΔZPE[e]	−2.2	−2.3	−2.0	−1.8	−1.6	−2.3	−2.5	−2.6	−1.8	−2.0
ΔZPE[f]					−3.5					−4.0

[a] In kcal mol^{-1}. [b] Adding suitable ΔZPE contribution leads to critical barrier E_0/kcal mol^{-1}. Where rotational isomers are possible (1,4- and 1,5-H-shift), barriers were calculated with respect to the linear chain conformation of 1-pentyl and 2-pentyl. [c] From AM1 level and scaled by 0.952; see ref 42. [d] From UMP2/6-311G** scaled by 0.9748; see ref 42. [e] From UMP2/6-311++G** scaled by 0.9748. [f] Scaling factor 0.9195 as used by default in G2MP2 theory. [g] For details concerning the additional values included in columns R5 and R7, see text.

where $V_a^G(s^{CVT})$ is the value of the adiabatic potential at the bottleneck. The extension of the numerator integral up to infinity ensures that the quantum correction on the reaction coordinate motion takes account of tunneling when the energy of the system is below the adiabatic threshold and of nonclassical reflection for energies above the barrier.[36,37] To obtain a realistic value of the transmission coefficient, especially at low temperatures, the transmission probabilities, $P(E)$, must be calculated. These depend on the effective mass of the system via the imaginary action integral as explained elsewhere.[37] The energy that dominates the integral in eq 6 as a result of the competition between the Boltzmann factor and $P(E)$ is known as the representative tunneling energy at a specific temperature. The most computationally intensive part of the calculation of the transmission coefficients is the evaluation of the adiabatic potential and the effective reduced mass which require knowledge of the Hessian, turning points and their derivatives, the eigenvector, and the curvature components $B_{mF}(s)$. The total curvature[38] defined as

$$\kappa(s) = [\sum_{m=1}^{F-1} (B_{mF})^2]^{1/2} \qquad (7)$$

is partitioned between different modes (m) and controls the nonadiabatic flow of energy between these modes and the reaction coordinate (F). Reaction path curvature effects included in the calculation of the transmission coefficients through $P(E)$ allow a qualitative understanding of the possible vibrational excitation of some of the modes in reactant or product.

In view of the large number of Hessians which are required, the dynamics calculations are based upon the VTST-IOC (variational transition state theory with interpolated optimized corrections) scheme developed by Hu et al,[39] and is one of the dual-level direct dynamics techniques. Two steps are involved. The calculation of the MEP is first carried out at a low level of theory, in our case the semiempirical AM1 model. Higher level ab initio data are then obtained for the stationary points and used to scale the low level data. We employed the UMP2/6-311G** geometries, frequencies and moments of inertia and PUMP-SAC2/6-311G** energies of the stationary points. Following the nomenclature of Truhlar et al. the dual-level dynamics model will be denoted PUMP-SAC2/6-311G**/// AM1.

In this work, thermal rate constants were calculated using both TST and CVT, and MEP calculations were performed in mass-weighted curvilinear coordinates (scaling mass set to 1 amu) with a step size of $0.01a_0$ for a total of 650 steps using the Page−McIver integrator. This step size was found to be sufficiently small to converge the reaction path and the transmission probabilities in the range $s = -3.5a_0$ to $s = +3.0a_0$ for the decomposition reactions and $s = -2.0a_0$ to $s = +2.0a_0$ for the isomerization reactions. To model vibrations transverse to the reaction path, we used curvilinear coordinates based on bond stretches, valence angle bends and bond torsions. Such coordinates are considered to better describe the GTS vibrations while rectilinear Cartesian coordinates are known to sometimes give a physically incorrect picture of the valence forces so that GTS low frequencies may become imaginary at certain points on the path.[40]

3. Electronic Structure Calculations

Prior to the present work, electronic structure calculations have been used to study β-CC scission and 1,3- and 1,4-H atom transfer in some primary alkyl radicals.[41] In our work, the following eight unimolecular pathways were modeled:

		$\Delta H_{298.15}$ (kcal mol^{-1})
$^{\bullet}CH_2CH_2CH_2CH_2CH_3 \rightarrow CH_3CH^{\bullet}CH_2CH_2CH_3$	(R1)	−2.1
$\rightarrow CH_3CH_2CH^{\bullet}CH_2CH_3$	(R2)	−1.7
$\rightarrow CH_3CH_2CH_2CH^{\bullet}CH_3$	(R3)	−2.1
$\rightarrow CH_3CH_2CH_2CH_2CH_2^{\bullet}$	(R4)	0.0
$^{\bullet}CH_2CH_2CH_2CH_2CH_3 \rightarrow {}^{\bullet}CH_2CH_2CH_3 + C_2H_4$	(R5)	25.7
$\rightarrow H + C_5H_{10}$	(R6)	28.3
$CH_3CH^{\bullet}CH_2CH_2CH_3 \rightarrow {}^{\bullet}CH_2CH_3 + C_3H_6$	(R7)	24.6
$\rightarrow H + C_5H_{10}$	(R8)	27.8

Here reactions R1−R4 are isomerizations of 1-pentyl and R5−R8 are C−C and C−H dissociation of the primary and secondary radical. The reaction enthalpies quoted above were derived from data calculated at the PUMP2/6-311G** level. In the calculation of the barriers, scaling factors defined for various models by Scott and Radom[42] have been applied for ZPEs and individual harmonic frequencies. The results are collected in Table 1, and selected geometrical parameters of the reactants, products and transition states are given in Figures 1 and 2.

The equilibrium geometry of the primary radical is similar to that reported by Pacansky et al.[2] and more recently by Viskolcz et al.[41] We use the same nomenclature as Pacansky et al. for the definition of the C−C bonds in alkyl radicals. Thus the α-CC bond includes the radical center, and the β-CC bond contains the carbon atom adjacent to the radical center and its next neighbor. The global energy minima of the normal radicals

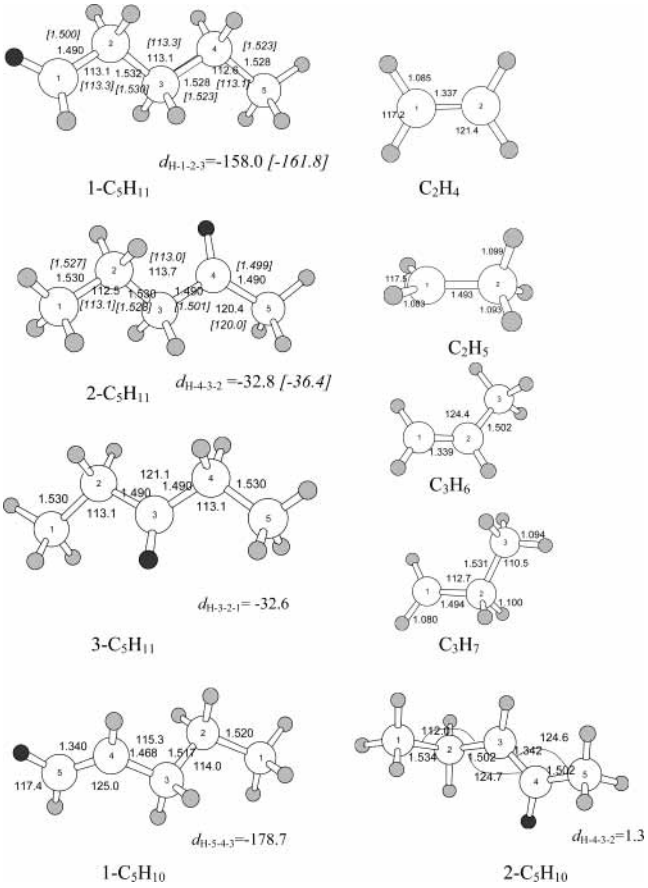

Figure 1. Selected geometric parameters for the equilibrium structures of the reactants and products for channels 1−8, as located on the PES at the UMP2/6-311G** [(CASSCF(3,3)/6-311G**)] level. Bond distances are in angstrom; bond angles and the dihedral angles are in degrees. The H atom in black is part of the quoted dihedral angle. For values of the C−H bonds see text.

have the carbon atoms arranged in a zigzag configuration. Semiempirical and ab initio calculations predict different conformations of the radical center at the end of the molecular chain. The UMP2/6-311G** optimized structures show that the radical center on the terminal C-atom (C1) is slightly distorted giving a pyramidal structure. Also, two distinct minima are located at this level of theory upon rotation about the α-CC bond, namely β_{CH} and β_{CC} conformers. For all theoretical models used in this study, the energy difference between the minima corresponding to β_{CH} and β_{CC} conformers of 1-pentyl radical was about 0.07 kcal mol^{-1}, the former being the most stable and thus considered the reference structure for the estimation of the barrier heights. An inspection of the 1-pentyl geometry at the UMP2/6-311G** level shows that the C(3)−C(4) and C(4)−C(5) bonds are of similar length (1.528 Å) whereas the perturbed bond (β-CC) is slightly longer. Such elongation is a common feature in normal and branched radicals and is an early indication of the most probable site for homolytic fragmentation.

Two other species formed during the isomerization processes are the secondary radicals, 2-pentyl and 3-pentyl, in which the radical center is C(2) and C(3), respectively (Figure 1). In 2-pentyl, we find that the C(3)−C(4) and C(4)−C(5) bond lengths are equal (1.49 Å) and the C(3)−C(4)−C(5) bond angle increases from 112.6° in 1-pentyl, to 120.4°, whereas in the symmetric 3-pentyl isomer the shortest bonds are α-CC (C(2)−C(3) and C(3)−C(4)), which include the radical center C(3). For all isomers, 1-pentyl, 2-pentyl, and 3-pentyl, the C−H bond lengths are similar. Their values are reported selectively since no important variation occurs. We mention only values for the α_{CH} bond lengths that increase from 1.083 Å in 1-pentyl to 1.088 Å in 2-pentyl, whereas the β_{CH} distances vary between 1.097 and 1.104 Å.

For the 1-pentyl system, the barriers for internal rotation about the α- and β-CC bonds are of interest. Pacansky et al.[2] reported the full torsional potential about α-, β-, and γ-CC bonds for the 1-hexyl radical as an illustrative example and noted that the torsional potential generated by the UMP2/6-31G* and UHF/6-31G* models were quantitatively the same leading to a barrier of 2.5 kcal mol^{-1} for the first conformational interconversion. In our study a similar rotation in 1-pentyl is required for the optimal steric orientation that leads to cyclization via TS(1,4) and TS(1,5) (Figure 2). We found that the PUMP2/6-311G** level of theory predicted a barrier of ∼3.0 kcal mol^{-1} in good agreement with previous quoted result. However by changing the level of theory from the semiempirical AM1 model to correlated PUMP-SAC2, the barrier for the internal rotation about β-CC bond increases by 50%.

3.1. Transition States for C−C Scission and Isomerization. For the thermal decomposition of normal and secondary pentyl, the actual reaction channels at high temperature are reactions R5 and R7. For completeness we have also examined the less favorable unimolecular dissociation pathways leading to H + alkene (reactions R6 and R8). The heats of reaction for (R5) and (R6) were found to be similar to those for C−C and C−H bond breaking in C_3-C_4 radicals where the branching fraction for the reaction corresponding to (R6) is small.[22]

Turning now to C−C bond scission, the calculated UMP2/6-311G** structures of the productlike transition states TS(dec1) and TS(dec2) (Figure 2) show that the breaking bond has increased in length by 47% and 46%, respectively, compared to the parent radicals, and the transition states occur late on the potential energy surface, characteristic of endothermic reactions. The lengthening of the β-CC bond is combined with a shortening of the α-CC bond in TS(dec1) or TS(dec2). As already mentioned in Section 2, the UHF wave functions for the saddle points TS(dec1) and TS(dec2) suffer a higher spin contamination. The data shown in Figure 2 for these two specific structures reveal that the use of single-reference UHF wave functions for the UMP2 geometry optimization did not have a significant effect on the predicted structures. The CASSCF(3,3)/6-311G** optimized structures are similar to UMP2/6-311G** ones, the only differences of significance are that the bonds being broken (of interest in dynamics) are shorter by some 0.03 Å at the CASSCF level. Since the differences are minor, we use the harmonic frequencies predicted at the UMP2 level for ZPE and thermal correction when necessary. We notice a few differences in the classical barriers (ZPE not included) according to the level of theory used. The highest barrier is predicted by the AM1 model for both reactions R5 and R7. The results which include electron correlation at the MP2 level and those from all three PUMP2 models agree closely within 0.3 kcal mol^{-1}. The lowest barrier for reactions R5 and R7 is predicted at the PUMP-SAC2/6-311G** level and slightly favors reaction R7, in agreement with experiment for smaller radicals at moderate temperatures.[8] In passing, we also describe results from G2-(MP2) and G2(PMP2) schemes, where PMP2 denotes the inclusion of projected UMP2 energy values in the original formulation of G2(MP2). The barrier heights are lower by some 0.8 and 0.5 kcal mol^{-1} for (R5) and (R7), respectively, but are generally in good agreement with the computationally less

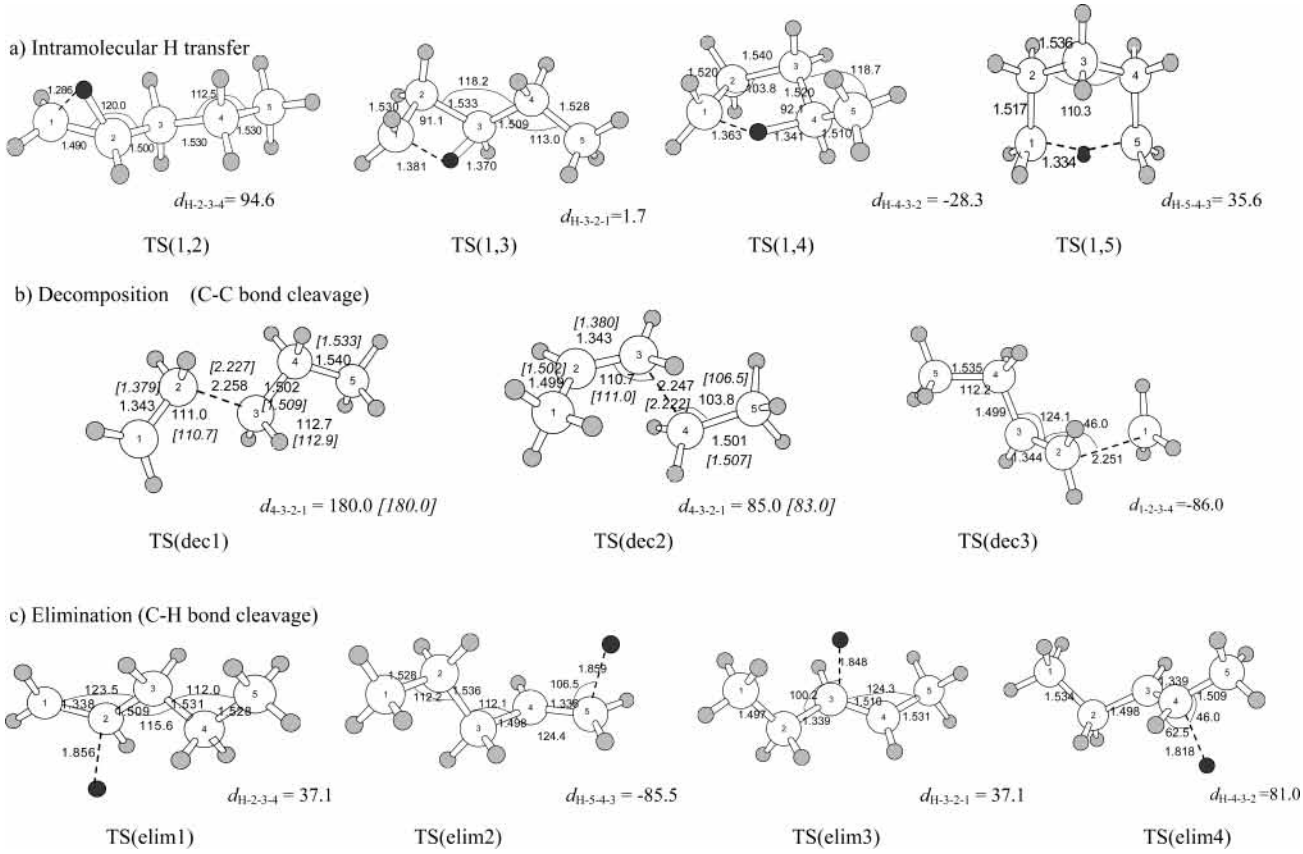

Figure 2. Selected geometric parameters for the transition state structures for the unimolecular isomerization and decomposition reactions in 1-pentyl system. Bond angles in angstrom and angles in degrees are given as obtained at the UMP2/6-311G** [(CASSCF(3,3)/6-311G**)] level of theory (transferring H atom in black).

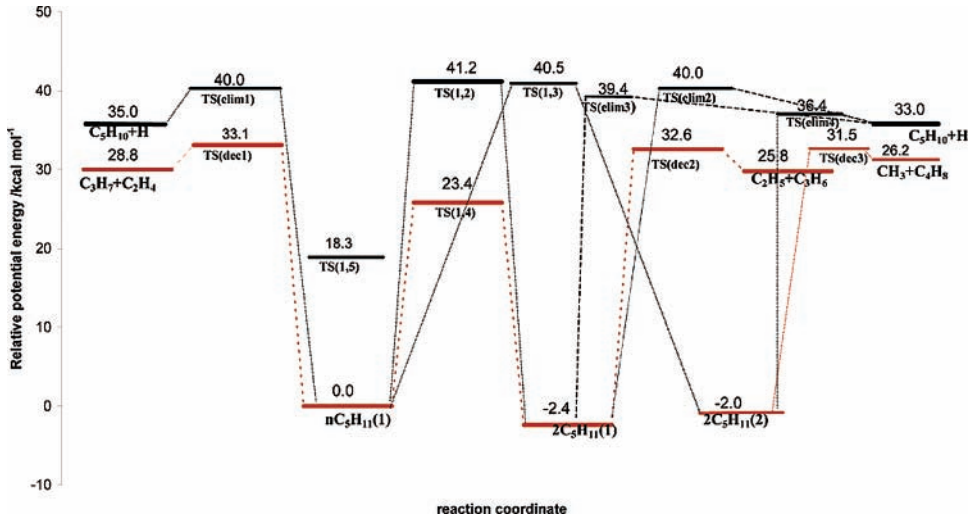

Figure 3. Overall potential energy surface (rotational isomers not included) calculated at the UMP2/6-311G** level of theory. Numbers denote the potential energy with respect to the 1-pentyl radical and do not include zero-point energy.

expensive PUMP-SAC2/6−3111G** level which is used in further dynamics calculations.

1-Pentyl and 2-pentyl radicals can in principle eliminate atomic hydrogen to form 1- or 2-pentene, the corresponding barriers being 40.0 and 39.4 kcal mol^{-1} at UMP2/6-311G** level, respectively. The lowest classical barrier for hydrogen elimination is actually found for the H elimination from 3-pentyl radical. Thus, TS(elim4) lies 3 kcal mol^{-1} below TS(elim3), but the occurrence of such a pathway is limited by the small probability of 3-pentyl formation, via a 1,3-H shift (Figure 3). The C−C and C−H dissociation reactions of 3-pentyl are not discussed further due to their unimportance in the 1-pentyl reaction system although we have calculated the relevant PES.

Symmetrical isomerization reactions of ethyl, 1-propyl, 1-butyl, and 1-pentyl radicals have been described theoretically by Viskolcz et al.[41] These reactions are thermoneutral but the barriers are expected to be representative for each class of reaction and provide a source of comparison with the present calculations. The four possible intramolecular H-transfers in 1-pentyl are represented by reactions R1−R4. Our calculated cyclic transition state structures (Figure 2) and energetics (Table 1) reflect the greater strain in the smaller ring. At the UMP2/

TABLE 2: Comparison of the Theoretical Threshold Energies (kcal mol^{-1}) (ZPE Corrected Barrier Heights) for Prototype Isomerization Reactions in Normal and Branched Radicals

type of process	1,2-H	1,3-H	1,4-H	1,5-H	ref
thermoneutral (*n*-alkyl radical)[a]	41.1	41.6	24.6	17.2	41
exothermic (1-pentyl radical)[b]	37.0	36.0	19.1	14.2	*e*
exothermic (*n*-alkyl radical)[c]	38.6	38.1	21.5	14.6	22
exothermic (branched alkyl radical)[d]	36.5	38.1	20.6	13.5	4

[a] MP−SAC2//UHF/6-31G* results. [b] This work at PUMP−SAC2//UMP2/6-311G**. [c] TST calculations and RRKM fit to experiment for 1,4-H was found to be the 20.5 ± 1.2 kcal mol^{-1} value subsequently corrected to reproduce low-temperature measurements. [d] MP−SAC2/6-311G**//UHF/6-31G*. [e] This work.

6-311G** level the length of the C−H bond being broken is the shortest for the three-membered cyclic structure (1.286 Å) but gradually increases up to 1.370 Å in the six-membered transition state. There is also more flexibility in the larger rings. Thus TS(1,2) is planar whereas the rings in TS(1,3), TS(1,4), and TS(1,5) are twisted to some degree, the corresponding dihedral angles being shown in Figure 2. As expected, the largest threshold energy (zero-point corrected barrier height) is obtained for the 1,2-H shift and is lowest for the 1,5-H transfer, in good agreement with previous theoretical work on the prototype isomerization reactions in straight chain and branched alkyl radicals as displayed in Table 2. Within a class of reaction (the corresponding transition state contains the same number of atoms including H-atoms) the barrier height changes both due to the presence of the substituents and the change of the heat of reaction. For instance the barrier height for the 1,2-H shift lies between 41.1 and 36.5 kcal mol^{-1}, the lowest value corresponding to the exothermic process, taking place in a branched alkyl radical. This suggests that by replacing the H atoms attached to the C atoms participating in the transition structure with alkyl groups, the barrier is lowered by 4.6 kcal mol^{-1}. A similar trend holds for each of the isomerization reactions. Our calculations at various levels of theory show there is a significant variation in the predicted barrier, the average value of the classical barrier being 39.9 ± 0.9, 39.8 ± 0.6, 22.8 ± 1.0 and 17.4 ± 1.0 kcal mol^{-1} for 1,2-, 1,3-, 1,4-, and 1,5-H atom transfer reactions, respectively.

4. Dynamics Calculations

4.1. Dissociation reactions. The calculated high-pressure limiting rate coefficients for β-CC bond scission are given as Arrhenius plots in Figure 4a. The flat potential energy surface is characteristic for both reactions R5 and R7, at single and dual-level, and a significant variational effect is reflected by the differences between the conventional transition state rate constants, k^{TST}, and canonical variational transition state rate constants, k^{CVT}. The displacement of the dynamical bottleneck from the location of the saddle point depends on temperature and is shifted to the reactant side for both reactions (Table 3). The ratio k^{CVT}/k^{TST} decreases more rapidly with temperature for reaction R5 reaching a value of 0.68 at 2000 K. The dual-level direct dynamics model predicts that the variational transition state is tighter than the saddle points TS(dec1) and TS(dec2), and the shift from about $-0.1a_0$ at 298 K to $-0.4a_0$ at 2000 K corresponds to a shortening of ∼ 0.08 Å in the C···C distance and a change in V_{MEP} of 0.5 kcal mol^{-1}. In this region, the adiabatic curve (Figure 5, parts a and b) is still flat and lies ∼0.4 kcal mol^{-1} below the saddle point. Such a small variation, due to local ZPE (see eq 5), indicates that the entropic factor becomes important as the temperature increases. The

TABLE 3: Bottleneck Properties[a,b] as a Function of Temperature for Reactions R3, R5, and R7

	reaction					
	1,4-H shift (R3)		C−C dissociation (R5)		C−C dissociation (R7)	
T (K)	s^{CVT}	V_a^G	s^{CVT}	V_a^G	s^{CVT}	V_a^G
	(a) Single Level AM1					
298.0	0.02	114.6	−0.13	124.9	−0.10	125.7
400.0	0.02	114.6	−0.14	124.9	−0.10	125.7
800.0	0.03	114.5	−0.24	124.7	−0.17	125.6
2000.0	0.05	114.5	−0.45	124.0	−0.36	125.2
	(b) Dual-Level PUMP−SAC2/6-311G**///AM1					
298.0	0.02	105.5	−0.12	119.4	−0.09	118.6
400.0	0.03	105.4	−0.14	119.4	−0.10	118.6
800.0	0.04	105.4	−0.26	119.3	−0.23	118.5
2000.0	0.06	105.3	−0.45	118.9	−0.30	118.2

[a] Value of the reaction coordinate, s, in amu bohr$^{1/2}$, scaling mass = 1 amu. [b] V_a^G in kcal mol^{-1}.

endothermic C−C dissociation reactions are characterized by loose and late transition states with an elongated C···C bond. The breaking C···C bond is 2.258 and 2.247 Å in TS(dec1) and TS(dec2), respectively and makes the bending motion of the C−C···C fragment very loose. The only generalized normal-mode frequencies significantly modified (at 298 K) at the new location of the CVT are the C−C−C bending mode (196 cm^{-1} in TS(dec1) and 203 cm^{-1} in TS(dec2)) and the $-CH_2$ rocking (607 cm^{-1} in TS(dec1)) and twisting modes (600 cm^{-1} in TS-(dec2)). These low frequencies affect the value of the entropic term of the CVT free energy of activation.[43] As the temperature increases from 298 to 2000 K the C−C−C bending frequencies increase by about 40 cm^{-1} and the $-CH_2$ rocking and twisting modes by 82 and 61 cm^{-1}, respectively. Thus the bending motion is slightly tightened and contributes to the CVT shift on the reactant side.

The magnitude of the tunnel correction may be calculated from the detailed numerical data given as Supporting Information (Table 1S). From the shape of the adiabatic ground-state potential V_a^G (s) along the MEP (Figure 5) we conclude that the interpolation technique yields a lower barrier but changes in the barrier profile are insignificant. The representative tunneling energy at 400 K, quoted in Figure 5, parts a and b, is only 0.01 kcal below the top of the adiabatic barrier (V^{AG}), for both 1-pentyl and 2-pentyl, clearly indicating that small curvature tunneling paths are insignificant, even at the lowest temperature considered in this study. The magnitude of the lowest generalized frequency changes along the reaction path indicates that internal rotation may assist the motion toward the saddle point but it is not involved in tunneling. The tunneling correction at 400 K is about 1.1 from both ZCT and SCT approximations for reactions R5 and R7 and converges to unity above 400 K.

4.2. Isomerization. We turn now to the intramolecular H transfer. The motion along the MEP can be pictured as occurring in three stages: in the reactant valley it corresponds to the stretching vibration of the C−H bond which is about to break, near the saddle point it corresponds to motion of the transferring H atom toward the acceptor radical center, and in the exit valley, it includes the asymmetric umbrella motion of the newly formed CH_3 moiety and $-CH_2$ rocking vibrations. The isomerization reactions (1,2-, 1,3-, 1,4-, and 1,5-) are slightly exothermic and characterized by different threshold energies as given in Tables 1 and 2. The variational effect is practically negligible for the whole temperature range investigated in this study. The CVT transition state is located essentially at the saddle point so that

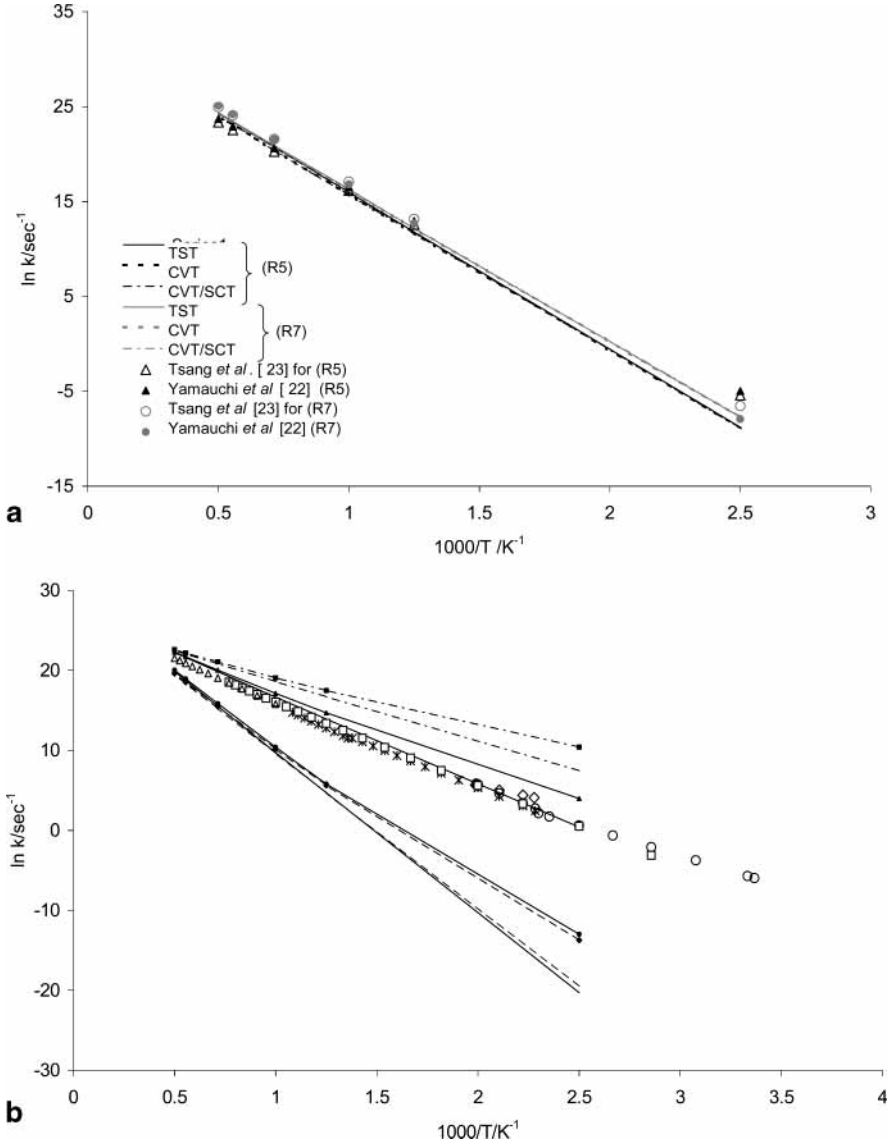

Figure 4. (a) Comparison of Arrhenius plots from TST (—), CVT (---), and CVT/SCT (-·-) for (R5) and (R7). (b) High-pressure limit rate constants as calculated using CVT(solid lines) and CVT/SCT(dashed lines with solid marks) for isomerization reactions R1 (—), R2(—), R3(---) and R4(-·-). Open symbols denote previous measurements for the 1,4-H shift by (◇) Endrenyi and LeRoy,[18] (○) Watkins,[46] (∗) Marshall,[45] (□) Yamauchi et al.,[22] and (△) Tsang et al.[24]

the CVT and TST rates are identical. Figure 6 (parts a−d) presents the shape of the adiabatic potential at the AM1 and dual-level (PUMP-SAC2/6-311G**///AM1) clearly indicating that the 1,2- and 1,3-H shifts depend greatly on tunneling at low temperature, the effect being assisted by the reduced width of the barrier and the low effective mass. This feature is also depicted in Figure 4b, where rate constants show a maximum increase of 2 orders of magnitude when SCT transmission coefficients are included (Table 2S). For such high barrier reactions, tunneling is more important than overbarrier motion up to 1000 K. The SCT transmission coefficients are almost twice the ZCT values below 1000 K. The reaction path curvature additionally plotted in Figure 6 shows a different profile from that for the decomposition reactions depicted in Figure 5. As a general feature there are two peaks symmetrically situated on each side of the saddle point. However, Figure 6a indicates a distinct behavior of the coupling terms (B_{mF} from eq 7) in the overall curvature (κ) for the 1,2-H shift. This is illustrated not only by the relative intensity of the two peaks but also by the location of each maximum at the end of the reaction path. To explain such differences, we investigated the GTS modes and find that an important contribution to the coupling operator comes from the C−H symmetric stretch and C(1)−H−C(2) bending mode. The large intensity of the peak on the exit channel is due to the contribution of the umbrella bending-mode in the terminal CH_3 moieties and additional backbone torsion. Transmission coefficients obtained in the SCT approximation increase the rate constants slightly for temperatures less than 1000 K on both surfaces (AM1 and dual level).

5. Comparison with Experimental and Theoretical Data

Experimentally measured values reported in the literature provide the primary source of data for comparison with the present results (Table 4). Existing kinetic data on reactions of interest for the 1-pentyl radical are compiled in Table 5 being mainly extracted from the NIST Chemical Kinetics Database[44] but also from several individual studies carried out more recently. We see that such data are widely scattered for each reaction, and are restricted to a certain range of temperature (and pressure) by the experimental method. Best results at temperatures above 1000 K are obtained in shock-tube experi-

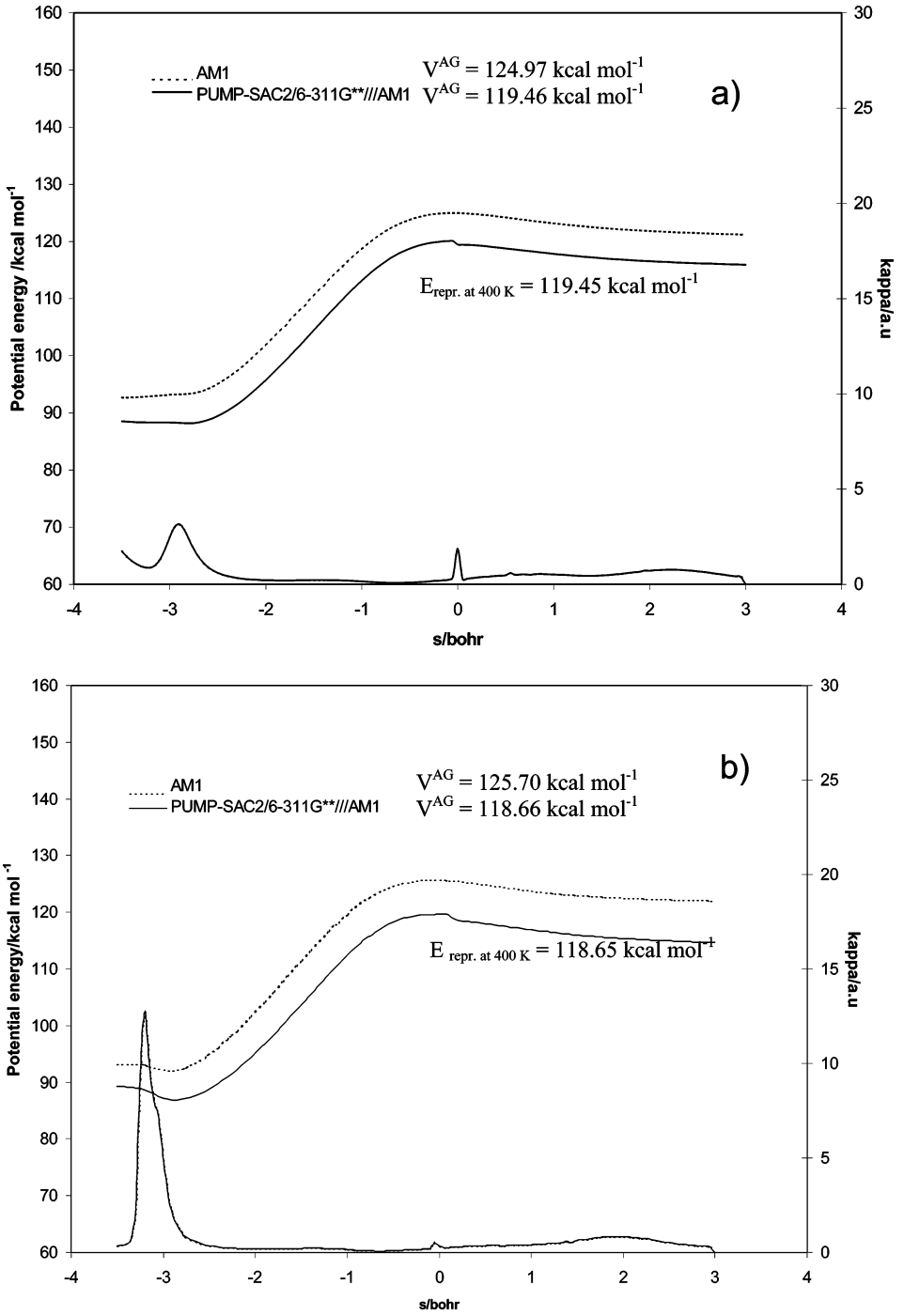

Figure 5. Plot of the adiabatic ground-state potential (V^{G}_{a}) (left scale) and the reaction path curvature (κ) for the C−C bond dissociation in a) 1-pentyl radical (reaction R5) and b) 2-pentyl radical (reaction R7).

ments with 10% accuracy. Estimation techniques can be used to calculate rate constants from structural features and rate parameters of reactions of smaller homologues,[23] but a more reliable estimation procedure is given by the ab initio calculations of the structures and energetics of the reaction coupled with variational transition state theory.

A critical evaluation of our present computational results is difficult as the experimental data are scarce and uncertainties are often not assigned. We note the considerable work on the 1,4-H-transfer reaction (reaction R3), where rate expressions for the high-pressure limit have been derived in terms of linear and nonlinear Arrhenius relationships. The Arrhenius parameters (E_a and A_∞) are scattered showing differences of about 1 order of magnitude in the preexponential factors (A_∞) and a maximum difference of 5 kcal mol^{-1} in the activation energy. These kinetic parameters were obtained from fitting over various temperature intervals and sometimes close to the falloff region. However, when two studies cover approximately the same temperature range (see Marshall[45] and Watkins[46]) the differences are a factor of 4 in the preexponential term and only 1 kcal mol^{-1} in the activation energy. Along with the literature values we show the kinetic parameters for the high-pressure limit as obtained from the linear fit of the dual-level CVT/SCT rate constant over the wider temperature range (400−2000 K) which is covered sparsely by experiment.

Two temperatures are commonly found in several studies, 400[18,22,45,46] and 1000 K,[22−24,45] and provide a good benchmark for comparison of the rate constants obtained in this study.

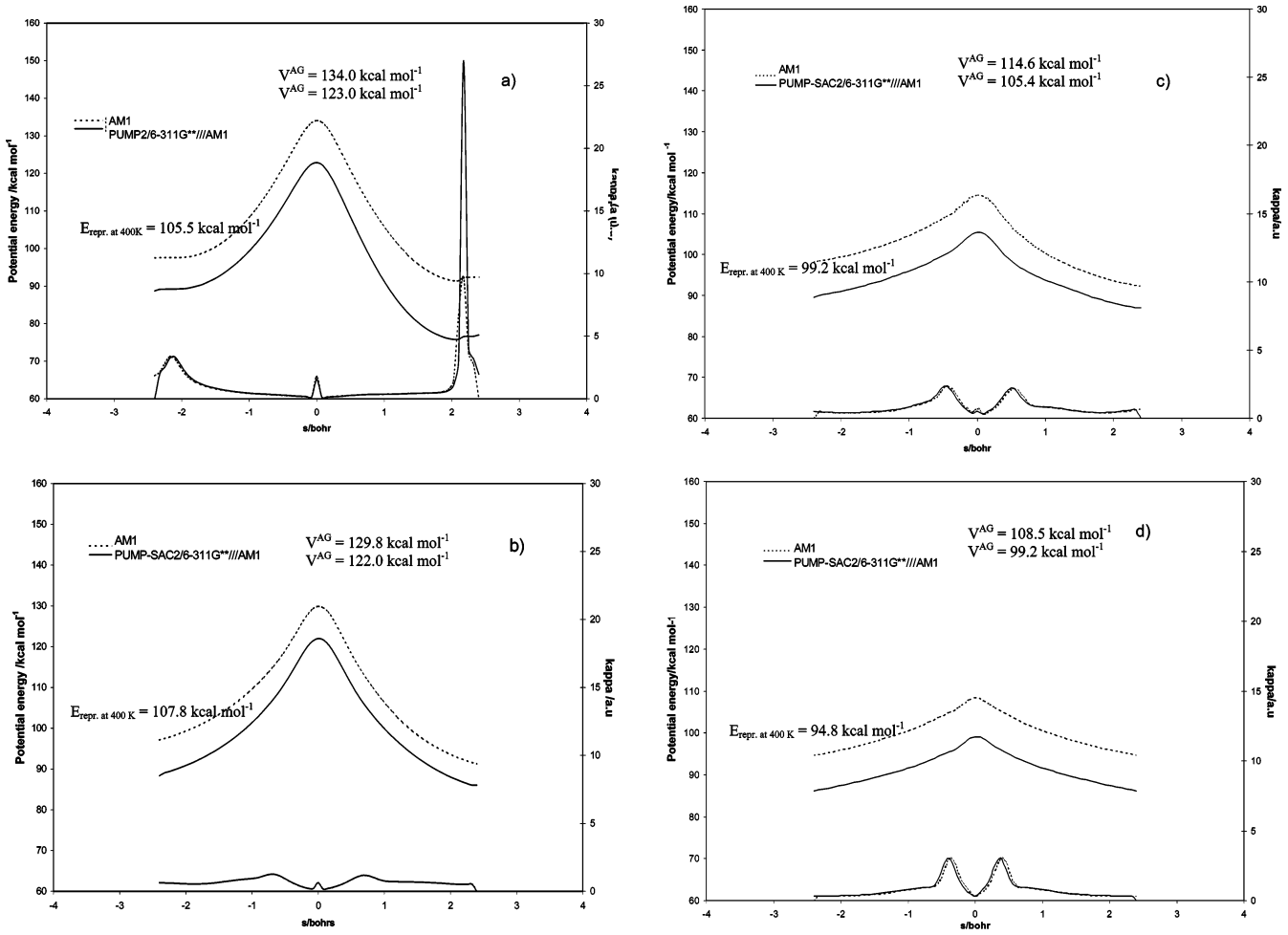

Figure 6. Plot of the adiabatic ground-state potential (V^{G}_{a}) (left scale) and the reaction path curvature (κ) as a function of the corresponding reaction coordinate *s*, at the AM1 (dashed curve) and UMP2/6-311G**///AM1 (solid curve) levels of theory for (a) 1,2-H shift, (b) 1,3-H shift, (c) 1,4-H shift, and (d) 1,5-H shift in 1-pentyl. Values for V^{AG} and s^{CVT} are quoted for the dual-level method.

TABLE 4: Arrhenius Parameters[a] Obtained from TST and CVT Including Tunneling for Reactions R3, R−3, R5, and R7

		A_∞ (s^{-1})			E_∞ (kcal mol^{-1})		
method		TST	CVT	CVT/SCT	TST	CVT	CVT/SCT
R3	AM1	1.8×10^{12}	1.8×10^{12}	1.2×10^{12}	22.7	22.6	20.9
	dual	1.4×10^{12}	1.3×10^{11}	9.2×10^{11}	20.2	20.2	18.1
R−3	AM1	4.8×10^{11}	4.5×10^{11}	3.1×10^{11}	27.9	27.8	26.0
	dual	8.7×10^{11}	8.6×10^{11}	5.8×10^{11}	22.5	22.5	20.5
R5	AM1	3.4×10^{14}	2.2×10^{14}	1.9×10^{14}	34.3	34.2	33.9
	dual	1.2×10^{14}	1.1×10^{13}	8.4×10^{13}	32.6	32.7	32.0
R7	AM1	1.8×10^{14}	1.0×10^{14}	7.5×10^{13}	35.1	34.8	34.5
	dual	8.2×10^{13}	6.9×10^{13}	5.5×10^{13}	31.8	31.9	31.1

[a] Arrhenius parameters obtained from linear fit of $k = A \exp(-E/RT)$ over the temperature range 400−2000 K.

Individual rate constants for R3 at 400 K calculated from the Arrhenius expressions of Endrenyi and LeRoy,[18] Watkins,[46] Marshall,[45] and Yamauchi et al.[22] are 59.5, 1.85, 16 and 1.65 s^{-1}. When a tunneling correction is included, we find $k_{CVT/SCT}^{400} = 53\ s^{-1}$, three times the value from Marshall's study and 10% smaller than the older value of Endrenyi and LeRoy. If a tunneling correction is not considered and we compare our value, $k_{CVT}^{400} = 1.5\ s^{-1}$ with values from Watkins[46] (1.85 s^{-1}) and Yamauchi et al.[22] (1.65 s^{-1}) the agreement is within a factor of 1.2. Such findings place our results within the uncertainty limit of 10 quoted by Marshall and the error limit of 3 indicated by Yamauchi et al., who did not consider tunneling in deriving their rate parameters. At 1000 K, our value, $k_{CVT/SCT}^{1000} = 2.7 \times 10^{7}\ s^{-1}$ is an order of magnitude greater that the value of $2.6 \times 10^{6}\ s^{-1}$ (Marshall) but is within a factor of 3 of the data from Yamauchi et al.[22] ($9.1 \times 10^{6}\ s^{-1}$), Tsang et al [24]($7.1 \times 10^{6}\ s^{-1}$), and Tsang et al.[23] ($1.2 \times 10^{7}\ s^{-1}$). We mention that the theoretical approach of Tsang et al.[24] to extract high-pressure limit rate parameters is different from ours in that they analyze a range of experimental data for related alkyl radical reactions followed by a RRKM fit and point out the degree of uncertainty in their data. In addition, they did not include tunneling corrections. Therefore, we are confident that our dual-level calculations yield rate coefficients consistent with previous theoretical work and with experimental data when uncertainties are taken into account.

The C−C decomposition reactions in 1-pentyl, (R5) and (R7), have been experimentally investigated in the high-temperature regime by Yamauchi et al.[22] and Tsang et al.[23] using shock-tube techniques. Despite the use of a similar technique the activation energies differ by 2.9 and 5.4 kcal mol^{-1} for (R5) and (R7), respectively. The fit of the linear Arrhenius expression to our dual-level CVT/SCT calculations for (R5) and (R7) yields preexponential factors of 8.4×10^{13} and $5.5 \times 10^{13}\ s^{-1}$ and gives corresponding activation energies of 32.0 and 31.1 kcal mol^{-1}. The A_∞ factors agree well with those of Yamauchi et al., but in contrast to their experimental finding, we predict the preferential channel for C−C cleavage to be reaction R7. If we compare our data with those of Tsang et al.,[23] there is an order

TABLE 5: High-Pressure Kinetic Parameters Available in the Literature for 1,4-H Isomerization and C−C Decomposition Reactions in 1-Pentyl System

reaction type	T (K)	technique	A (s^{-1})	E_a (kcal mol^{-1})	ref
1,4-H shift					
(R3)	297−453	DP+GC	3.3×10^8	15.1	16
	439−503	DP+KM	1.4×10^7	10.8	18
	438−502	reevaluation[a]	5.0×10^{11}	21.1	46
	438−923	S+GC	1.2×10^{11}	20.1	45
	737−923	F+GC	9.1×10^{11}	23.40 ± 2.1	45
	350−1300	ST+ARAS	$6.1 \times 10^{10}\ (T/298)^{0.85}$	19.5	22
	400−2000	DL-DD	9.2×10^{11}	18.1	*c*
	850−1000	ST+KM	1.0×10^{12}	22.5	23
	1000−2000	Meq-TST	7.0×10^{11}	22.9	24
C−C diss					
primary radical (R5)	400−2000	DL-DD	8.4×10^{13}	32.0	*c*
	1000−2000	Meq+TST	1.8×10^{13}	28.6	24
	1000−1300	ST+ARAS	1.8×10^{14}	31.3	22
	850−1000	ST+KM	1.0×10^{13}	28.4	23
secondary radical (R7)	400−2000	DL-DD	5.5×10^{13}	31.1	*c*
	1000−2000	Meq+TST	2.5×10^{13}	28.4	24
	1000−1300	ST+ARAS	3.0×10^{14}	32.8	22
	850−1000	ST+KM	8.0×10^{12}	27.4	23

[a] Based on thermochemical and kinetic data. [b] List of abbreviations related to experimental technique:S-static system, F-flow system, ST-shock tube, KM-kinetic modeling, DP-direct photolysis, GC-gas chromatography, ARAS-atomic resonance absorption spectroscopy, DL-DD-dual level direct dynamics, Meq-TST-Master equation and transition state theory. [c] This work.

of magnitude difference in the A factors and a consistent difference in activation energies of 4 kcal mol^{-1}. Also, $k_{CVT/SCT}^{800}(R5) = 1.7 \times 10^5\ s^{-1}$ is within 5% of the corresponding value of Tsang et al.[23] and is about half the corresponding value of Yamauchi et al.[22]

In conclusion, we have supplemented the experimental data with high-pressure limiting Arrhenius expressions based on molecular parameters, energetics, and thermochemical data obtained at an ab initio level. These values agree well with previous work and are derived over a wider temperature range. We are confident they will provide an accurate input into master equation models.

6. Conclusions

We have described a direct dynamics study on the thermal decomposition and isomerization reactions for the 1-pentyl system. The size of the system has allowed us to test various theoretical models in predicting the structures, activation barriers and reaction energetics and to carry out the dynamics with an accurate and yet computational affordable dual-level model. The results of the calculations can be directly included, with no tuning of parameters, in experimental databases. The main conclusions of our study are as follows:

(a) As expected, the activation energy for 1,4-isomerization is lower than that for β-CC bond cleavage.

(b) The use of conventional TST method overestimates the rate for C−C bond cleavage. The CVT method predicts a significant shift in the position of the dynamical bottleneck with increasing temperature. This is accompanied by substantial changes in the angular modes, so that application of the flexible transition state theory (FTST)[47] should lead to further refinement of the rate coefficient. Tunneling is shown to be negligible, a result of the large effective mass and the broad barrier. The A factors obtained in dual-level calculations are $8.4 \times 10^{13}\ s^{-1}$ for (R5) and $5.5 \times 10^{13}\ s^{-1}$ for (R7). The corresponding activation energies are 32.0 and 31.1 kcal mol^{-1}, ~3 kcal mol^{-1} higher than values previously reported.[22]

(c) The A_∞ factor for the forward 1,4-H transfer reaction in 1-pentyl obtained from the CVT/SCT dynamic model is $9.2 \times 10^{11}\ s^{-1}$, being fairly close to that for the 1,4-H shift in the 2-methylhexyl radical, for which Viscolcz et al.[4] has reported values in the range $9.8 \times 10^{11}-5.3 \times 10^{11}\ s^{-1}$, depending upon the carbon atom type (primary, secondary, tertiary), hosting the transferring hydrogen. Variational effects are unimportant in isomerization, because the barrier is narrow; tunneling, however, is very significant, especially at lower temperatures.

Although the present study provides a detailed description of the structures, energetics, and dynamics of the reactions of interest, it would be of value to achieve a comparable accuracy at lower computational cost. In a previous study on the decomposition of the 1-propyl radical, we reported a new set of parameters for the semiempirical AM1 method, denoted as the AM1-SRP2 model.[48] The reparametrization was done to improve the barrier height and reaction energy predicted for the C−C decomposition reaction. This AM1-SRP2 model was tested here to investigate the dynamics of β-CC scission in 1-pentyl (reaction R5). The geometry for the normal radical and for the corresponding transition state TS(dec1) are given as Supporting Information (Table 3S) along with energetic and kinetic data as obtained at AM1-SRP2 and UMP2/6-311G**/// AM1 levels.

The results indicate that the AM1-SRP2 model performs well as regards the structural parameters of the reactants and products when compared to the more computationally expensive UMP2/6-311G** method. However, the length of the breaking β-CC bond in TS(dec1) is underestimated by about 9%, showing a tighter saddle point than that predicted by the UMP2/6-311G** model, and the Arrhenius parameters are better predicted by the re-parametrized model than by the dual-level direct dynamics technique. We consider this result encouraging, but nevertheless, the AM1-SRP2 model must be thoroughly tested on homologous decomposition reactions of primary radicals to judge if it can be routinely applied to this class of reactions.

Acknowledgment. We thank the EPSRC for support and Professor D. G Truhlar for use of the Gaussrate code.

Supporting Information Available: Table 1S, giving rate constants/s^{-1}, for the β-CC bond dissociation in 1-pentyl (eq R5) and 2-pentyl (eq R7) for the temperature range 400−2000 K (first two columns displaing rate coefficients including tunneling corrections with ZCT and SCT models), Table 2S

giving rate constants/s^{-1}, for the isomerization reactions R1−R4 in the temperature range 400−2000 K (first two columns display rate coefficients including tunnelling corrections with ZCT and SCT models), and Table 3S giving selected geometric parameters for 1-pentyl, TS(dec1) and products ($C_3H_7 + C_2H_4$) at the AM1-SRP2 level and UMP2/6-311G**///AM1. This material is available free of charge via the Internet at http://pubs.acs.org.

References and Notes

(1) Walker, R. W.; Morley, C. Low-Temperature Combustion and Autoignition. In *Comprehensive Chemical Kinetics*; Pilling, M., Ed.; Elsevier: New York, 1997; Vol. 35, Chapter 1.

(2) Pacansky, J.; Waltman, R. J.; Barnes, L. A. *J. Phys. Chem*. **1993**, *97*, 10694.

(3) Ross, P. L.; Johnston, M. V. *J. Phys. Chem*. **1995**, *99*, 16507.

(4) Viskolcz, B.; Lendvay, G.; Seres, L. *J. Phys. Chem. A* **1997**, *101*, 7119.

(5) Sommnitz, H.; Zellner, R. *Phys. Chem. Chem. Phys*. **2000**, *2*, 1899.

(6) Hippler, H.; Striebel, F.; Viskolcz, B. *Phys. Chem. Chem. Phys*. **2001**, *3*, 2450.

(7) Kukui, A.; Le Bras, G. *Phys. Chem. Chem. Phys*. **2001**, *3*, 175.

(8) Knyazev, V. D.; Slagle, I. R. *J. Phys. Chem*. **1996**, *100*, 5318.

(9) Garrett, B. C.; Truhlar, D. G. *J. Phys. Chem*. **1983**, *87*, 4553.

(10) Truhlar, D. G.; Issacson, A. D.; Garrett, B. C. In *Theory of Chemical Dynamics*; Baer, M., Ed.; CRC Press: Boca Raton, FL, 1985; Vol. IV, Chapter 2, pp 65−138.

(11) Gilbert, R. G.; Smith, S. C. *Unimolecular and Recombination Reactions*; Blackwell: Oxford, U.K., 1990.

(12) Knyazev, V. D.; Tsang, W. *J. Phys. Chem. A* **2000**, *104*, 10747.

(13) Venkatesh, P. K.; Dean, A. M.; Cohen, M. H.; Carr, R. W. *J. Chem. Phys*. **1999**, *111*, 8313.

(14) Frankcombe, T. J.; Smith, S. C.; Gates, K. E.; Robertson, S. H. *Phys. Chem. Chem. Phys*. **2000**, *2*, 793.

(15) Barker, J. R.; Ortiz, N. F. *Int. J. Chem. Kinet.* **2000**, *33*, 246.

(16) Watkins, K. W. *J. Am. Chem. Soc*. **1971**, *93*, 6355.

(17) Watkins, K. W. *J. Phys. Chem*. **1973**, *77*, 2938.

(18) Endrenyi, L.; Le Roy, D. J. *J. Phys. Chem*. **1966**, *70*, 4081.

(19) Frey, H. M.; Walsh, R. *Chem. Rev*. **1969**, *69*, 103.

(20) Dearden, D. V.; Beauchamp, J. L. *J. Phys. Chem*. **1985**, *89*, 5359.

(21) Tardy, D. C. *Int. J. Chem. Kinet.* **1974**, *6*, 291.

(22) Yamauchi, N.; Miyoshi, A.; Kosaka, K.; Koshi, M.; Matsui, H. *J. Phys. Chem. A* **1999**, *103*, 2723.

(23) Tsang, W.; Walker, J. A.; Manion, J. A. *Symp. (Int.) Combust., [Proc]* **1998**, *27th* (1), 135.

(24) Tsang, W.; Bedanov, V.; Zachariah, M. R. *Ber. Bunsen-Ges. Phys. Chem.* **1997**, *101*, 491.

(25) Schmidt, M. W.; Gordon, M. S. *Annu. Rev. Phys. Chem*. **1998**, *49*, 233.

(26) Chen, W.; Schlegel, H. B. *J. Chem. Phys*. **1994**, *101*, 5957.

(27) Gordon, M. S.; Truhlar, D. G. *J. Am. Chem. Soc*. **1986**, *108*, 5412.

(28) Truong, T. N.; Truhlar, D. G. *J. Chem. Phys*. **1990**, *93*, 1761.

(29) Gordon, M. S.; Truhlar, D. G. *Int. J. Quantum Chem*. **1987**, *31*, 81.

(30) *Gaussian98*, Frisch, M. G.; Trucks, G. W.; Schlegel, H. B.; Gill, P. M.; Johnson, B. G.; Robb, M. A.; Cheeseman, J. R.; Keith, T.; Peterson, G. A.; Montgomery, J. A.; Raghavachari, K.; Al-Laham, M. A.; Zakrzwski, W. G.; Ortiz, J. V.; Foresman, J. B.; Cioslowski, J.; Stefanov, B. B.; Nanayakkara, A.; Challacombe, M.; Peng, C. Y.; Ayala, P. Y.; Chen, W.; Wong, M. W.; Andres, J. L.; Repongle, E. S.; Gomperts, R.; Martin, R. L.; Fox, D. J.; Binkley, J. S.; Defrees, D. J.; Baker, J. A.; Stewart, J. P. P.; Head-Gordon, M.; Gonzalez, C.; Pople, J. A. Gaussian Inc.: Pittsburgh, PA, 1995.

(31) *Gaussrate* v.8.0, Corchado, J. C.; Coitiono, E. L.; Chuang, Y. Y.; Truhlar, D. G. Department of Chemistry and Supercomputer Institute, University of Minnesota: Mineapolis, MN 55455−0431.

(32) Tucker, S. C.; Truhlar, D. G. In *New Theoretical concepts for Understanding Organic reactions*; Bertran, J., Csizmadia, I. G., Eds., Kluwer: Dordrecht, The Netherlands, 1989; pp 291−346.

(33) Truhlar, D. G.; Garrett, B. C. *Annu. Rev. Phys. Chem*. **1984**, *35*, 159.

(34) Garrett, B. C.; Truhlar, D. G.; Grev, R. S.; Magnunson, A. W. *J. Phys. Chem*. **1980**, *84*, 1730.

(35) Lu, D−h.; Truong, T. N.; Melissas, V. S.; Lunch, G. C.; Liu, Y. P.; Garrett, B. C.; Steckler, R.; Issacson, A. D.; Rai, S. N.; Hancock, G. C.; Lauderdale, J. C.; Joseph, T.; Truhlar, D. G. *Comput. Phys. Commun*. **1992**, *71*, 235.

(36) Garrett, B. C.; Truhlar, D. G. *J. Phys. Chem*. **1979**, *83*, 2921.

(37) Skodje, R. T.; Truhlar, D. G.; Garrett, B. C. *J. Phys. Chem*. **1982**, *77*, 5955.

(38) Page, M.; McIver, J. W., Jr. *J. Chem. Phys*. **1988**, *88*, 922.

(39) Hu, W. P.; Liu, Y. P.; Truhlar, D. G. *J. Chem. Soc., Faraday Trans*. **1994**, *90*, 1715.

(40) Natanson, G. A.; Garrett, B. C.; Truong, T. N.; Joseph, T.; Truhlar, D. G. *J. Chem. Phys*. **1991**, *94*, 7875.

(41) Viskolcz, B.; Lendvay, G.; Körtvélyesi, T.; Seres, L. *J. Am. Chem. Soc*. **1996**, *118*, 3006.

(42) Scott, A. P.; Radom, L. *J. Phys. Chem*. **1996**, *100*, 16502.

(43) Villa, J.; Gonzalez-Lafont, A.; Llunch, J. M.; Bertran, J. *Mol. Phys*. **1996**, *89*, 633.

(44) NIST Chemical Kinetics Database, Standard Reference Database 17, v.7.0 (web version), http://kinetics.nist.gov.

(45) Marshall, R. M. *Int. J. Chem. Kinet*. **1990**, *22*, 935.

(46) Watkins, K. W. *Can. J. Chem*. **1972**, *50*, 3738.

(47) Robertson, S.; Wagner, A. F.; Wardlaw, D. M. *J. Chem. Phys*. **2000**, *113*, 2648.

(48) Jitariu, L. C.; Wang, H.; Hillier, I. H.; Pilling, M. J. *Phys. Chem. Chem. Phys*. **2001**, *3*, 2459.